GEOPHYSICS, VOL. 77, NO. 1 (JANUARY-FEBRUARY 2012); P. Q15–Q25, 12 FIGS.
10.1190/GEO2011-0300.1

Suppressing nonphysical reflections in Green's function estimates using source-receiver interferometry

Simon King[1] and Andrew Curtis[2]

ABSTRACT

Seismic interferometry retrieves the Green's function propagating between two receiver locations using their recordings from an enclosing boundary of sources. Theory requires that sources completely surround the two receivers, but constraints in exploration seismology restrict sources to locations near the surface of the earth. Seismic interferometry by crosscorrelation then introduces usually undesirable nonphysical reflections (spurious multiples) in the Green's function estimates. We found that the dominant nonphysical reflections can be converted into physical reflections via convolution using source-receiver interferometry. The resultant Green's functions display fewer nonphysical reflections and show significantly better agreement with the true Green's functions than those obtained using crosscorrelational interferometry. Nonphysical reflections can be further suppressed by iterating the convolution step. By comparing the velocity spectra of the Green's functions retrieved by crosscorrelational and source-receiver interferometry, we can retrospectively identify the dominant nonphysical reflections introduced by crosscorrelational interferometry. We found that the nonphysical reflections are particularly important for constructing the primary reflections and internal multiples in source-receiver interferometry. This is because the primary reflections and internal multiples cannot be created via the convolution of physical reflections. Instead, the primary reflections and internal multiples are retrieved by the appropriate convolution between a nonphysical and physical reflection. We compared crosscorrelational interferometry and source-receiver interferometry using synthetic towed streamer data for a 1D acoustic and 2.5D elastic model, respectively. We also found that the nonphysical reflections obtained using crosscorrelational interferometry allow for the direct estimation of interval velocities and layer thicknesses without the need to use Dix inversion in the 1D example.

INTRODUCTION

Seismic interferometry refers to the process whereby the crosscorrelation (Wapenaar, 2004; van Manen et al., 2005, 2006; Bakulin and Calvert, 2006; Wapenaar and Fokkema, 2006), deconvolution (Vasconcelos and Snieder, 2008a, b; Wapenaar et al., 2008, 2011; van der Neut et al., 2011) or crossconvolution (Slob and Wapenaar, 2007; Slob et al., 2007) and integration of wavefields recorded at two receivers from an enclosing boundary of sources provides the Green's function that would be recorded at one receiver if the other receiver instead acted as a (so-called "virtual") source. By source-receiver reciprocity, Hong and Menke (2006) and Curtis et al. (2009) show that the Green's function between two sources can be estimated given their recordings on a surrounding set of receivers. Thus one of the sources acts as a virtual receiver. Similarly, Poletto and Farina (2010) show that the crossconvolution of the wavefields emitted by two seismic sources recorded at the boundary of the receivers provide the Green's function between the sources as if there was a virtual reflector at the boundary. Source-receiver interferometry outlined by Curtis and Halliday (2010b) combine these formerly independent Green's function re presentations (i.e., the virtual source and virtual receiver methods) to estimate the Green's function between a source and receiver pro-

Manuscript received by the Editor 9 August 2011; revised manuscript received 12 October 2011; published online 8 February 2012; corrected version published online 14 February 2012.
[1]The University of Edinburgh, Formerly School of GeoSciences, and Edinburgh Collaborative of Subsurface Science and Engineering (ECOSSE), Edinburgh, U. K.; presently Fugro Seismic Imaging, Swanley, U. K. E-mail: s.j.king@sms.ed.ac.uk.
[2]The University of Edinburgh, School of GeoSciences, and Edinburgh Collaborative of Subsurface Science and Engineering (ECOSSE), Edinburgh, U. K. E-mail: andrew.curtis@ed.ac.uk.

vided we have recordings of a surrounding set of sources also at a surrounding set of receivers.

In exploration seismology, many of the theoretical requirements in seismic interferometry are contravened. First, the dipolar sources required by the complete theory are usually unavailable. Wapenaar and Fokkema (2006) show that the Green's function can be retrieved by a single crosscorrelation of monopolar Green's functions under certain approximations. These include the assumption that sources are located on a circle with very large radius such that energy propagating from a source leaves the boundary approximately perpendicularly and that no energy is reflected back into the medium via scatterers outside of the boundary. Second, in crosscorrelational interferometry, the medium is usually assumed to be lossless despite the fact the earth is strongly attenuating. However, it has been shown that the electromagnetic (Slob and Wapenaar, 2007; Slob et al., 2007) and surface wave (Halliday and Curtis, 2008, 2009) Green's functions are recovered well in attenuative media by crossconvolutional interferometry and that the general Green's functions can be obtained by crosscorrelational interferometry only, if additional sources distributed throughout the medium compensate for the energy loss due to attenuation (Snieder, 2007). Third, theory requires we have a complete boundary of sources that surround the two receivers, but practicalities limit the illuminating sources to locations near or on the surface of the earth (so-called surface sources). When only surface sources are available, nonphysical reflections are produced in the Green's function estimates. These are formed by the crosscorrelation of reflections from different interfaces, and are called spurious multiples by Snieder et al. (2006).

Nonphysical reflections would cancel by destructive interference if the surface sources were supplemented by sources at depth (see Figure 14 in Snieder et al., 2006), or by wavefields which scatter back toward the receivers by a sufficiently inhomogeneous medium (Wapenaar, 2006). Nonphysical reflections can also be suppressed if we decompose the recorded wavefields prior to crosscorrelation. Bakulin and Calvert (2006) show that improved Green's function estimates between receivers in a horizontal well are obtained by crosscorrelating the full wavefield Green's function with the time-windowed direct arrivals at the virtual source. Mehta et al. (2007) instead perform up/down decomposition at ocean-bottom receivers, which allows the upgoing wavefield to be crosscorrelated with the time-windowed downgoing direct arrivals. The physical reflections are well recovered in both methods because crosscorrelational seismic interferometry essentially removes the common component of the reflection that passes through both receivers (Figure 1a). The source in Figure 1a, which provides the dominant contribution to the Green's function estimate, is referred to as a stationary-phase source. For a mathematical derivation of stationary phase, the reader is referred to Snieder et al. (2006), who determine the position of the stationary-phase sources for the primary reflections between the receivers. Also, by omitting the reflected wavefields from Green's functions at $\mathbf{x}_A$ for example, the methods of Bakulin and Calvert (2006) and Mehta et al. (2007) do not produce crosscorrelations between different reflections, and thus unwanted nonphysical reflections are suppressed.

The suppression methods of Bakulin and Calvert (2006) and Mehta et al. (2007) are only applicable when receivers are positioned vertically beneath surface sources (e.g., Figure 1a). However, these methods fail to recover the physical reflections when receivers are positioned adjacent to surface sources as in towed streamer recordings. In that case the direct arrival travels horizontally along the receiver array and hence does not share a common component of the recorded reflections as demonstrated in Figure 1a. For this reason the Green's functions are best obtained in towed streamer data by crosscorrelating the reflections at both receivers (van Wijk, 2006). For example, Schuster et al. (2004) show that the crosscorrelation of a first-order free-surface multiple with a ghost reflection isolates the Green's function kinematically equivalent to the primary reflection between the two receivers (Figure 1b). Such a formulation allows the physical components of Green's functions to be constructed, but unfortunately introduces the undesirable nonphysical reflections as described above.

It has recently been observed in a field data set that interreceiver Green's function estimates obtained using source-receiver interferometry theory were of better quality than those obtained by crosscorrelational or crossconvolutional interferometry (Duguid et al., 2011). To date, no explanation of why this should be the case has been proposed. In this paper we show that the dominant nonphysical reflections obtained using sources and receivers in a towed streamer configuration from crosscorrelational seismic interferometry, can be used constructively in source-receiver interferometry to obtain Green's function estimates with fewer nonphysical reflections. The approach is similar to that of Ikelle et al. (2009) who use crosscorrelation and crossconvolution to construct internal multiples. However, we propose that the crosscorrelation and crossconvolution can be used to construct complete Green's functions with fewer nonphysical reflections. Essentially, source-receiver interferometry includes a step that allows many of the nonphysical reflections to be converted back into physical reflections via convolution. In this instance we use a modified version of source-receiver interferometry, which we will describe in the next section to obtain Green's functions between receivers only. Hence, there are good

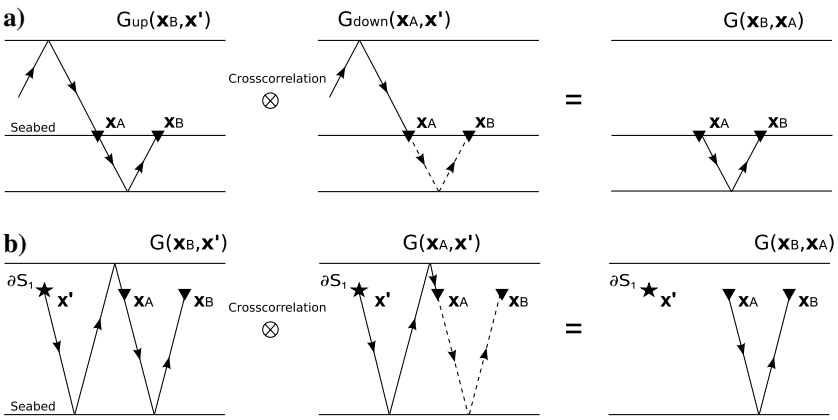

Figure 1. (a) Crosscorrelation of the upgoing Green's function recorded at $\mathbf{x}_B$ (left) with the downgoing Green's function recorded at $\mathbf{x}_A$ (middle) isolates the traveltime of the primary reflection between the receiver locations (right). The common portion of the reflection which is annihilated in this case is the direct arrival recorded at $\mathbf{x}_A$. (b) Crosscorrelation of the first-order free-surface multiple at $\mathbf{x}_B$ (left) with the ghost reflection at $\mathbf{x}_A$ (middle) isolates the traveltime of the primary reflection between the receiver locations (right).

theoretical reasons why source-receiver interferometry might outperform crosscorrelational interferometry in some situations. Although this may not provide a full explanation of the results of Duguid et al. (2011), it does provide a basis with which we might expect the quality improvement to be observed in more general applications of source-receiver interferometry.

In the next section we outline crosscorrelational and source-receiver interferometry and describe the methodology whereby nonphysical reflections can be used constructively in source-receiver interferometry to produce physical reflections. We demonstrate the phenomenon on a 1D acoustic model and subsequently on a 2.5D model based on a North sea oilfield. We finish by discussing the implications and limitations of this work.

METHODOLOGY

To avoid the requirement for both monopolar and dipolar sources, Wapenaar and Fokkema (2006, p. SI37–SI38) show that if sources lie in the far-field of the receivers, the Green's function $G(\mathbf{x}_B, \mathbf{x}_A)$ between two receivers positioned at $\mathbf{x}_A$ and $\mathbf{x}_B$ plus its complex conjugate is approximated by the crosscorrelation of wavefields from only monopolar sources:

$$G(\mathbf{x}_B, \mathbf{x}_A) + G^*(\mathbf{x}_B, \mathbf{x}_A) \approx \oint_{\partial S_1} \frac{2}{\rho c} G(\mathbf{x}_B, \mathbf{x}') G^*(\mathbf{x}_A, \mathbf{x}') d^2\mathbf{x}', \quad (1)$$

where ρ and c are the density and velocity, respectively, and are assumed to be constant at each source positioned at $\mathbf{x}'$ on a boundary ∂S_1. The dependence on frequency ω is omitted to simplify the notation. The Green's functions on the right-hand side represent pressure responses at the receiver locations $\mathbf{x}_A$ and $\mathbf{x}_B$ from impulsive pressure sources at $\mathbf{x}'$. Assuming the Green's functions are excited by a source wavelet $s(\omega)$, e.g., $s(\omega)G(\mathbf{x}_A, \mathbf{x}')$, the right-hand side of equation 1, would, in theory, include the power spectrum of the source wavelet $|s(\omega)|^2$. Integrating the crosscorrelations over the total number of sources (closed integral in equation 1) isolates the Green's function $G(\mathbf{x}_B, \mathbf{x}_A) + G^*(\mathbf{x}_B, \mathbf{x}_A)$ as though a source was fired at $\mathbf{x}_A$ and the response recorded at $\mathbf{x}_B$. Equation 1 is the simplified acoustic approximation in seismic interferometry.

We showed in Figure 1 for a simple 1D medium that crosscorrelational interferometry (equation 1) removes the traveltime associated with the common component of the wavefield that passes through both receivers, resulting in waves that have the traveltimes of physical reflections. However, the same process synthesizes waves with the traveltime of a nonphysical reflection by crosscorrelation of the primary reflection from two different interfaces, for example, the primary reflection from the second interface recorded at $\mathbf{x}_B$ crosscorrelated with the primary reflection from the first interface recorded at $\mathbf{x}_A$ (Figure 2a). The nonphysical reflection can be intuitively interpreted as the wavefield reflected from the second interface as though the virtual source and receiver were positioned at the first interface. As shown in the right-hand side of Figure 2a, the retrieved Green's function is positioned to the left of the two receivers. However, in a laterally invariant medium the retrieved Green's function could just as well be shifted to the right to represent the reflection propagating directly between the receivers. The crosscorrelation between the primary reflection from the third interface with the primary reflection from the second interface provides the traveltime of a nonphysical reflection corresponding to a reflection propagating through the third layer only (Figure 2b). A nonphysical reflection that propagates through two layers is provided by the crosscorrelation of the primary reflections shown in Figure 2c. What can be observed immediately, is that some of these nonphysical reflections are sensitive only to the velocity within a single layer (Figure 2a and 2b). We will investigate this property below to provide a new velocity analysis method that uses nonphysical reflections to identify individual layer velocity directly, without the need for Dix inversion (Dix, 1955).

Ikelle et al. (2009) term these nonphysical reflections virtual events and provide a different interpretation of the reflections on the right-hand side of Figure 2. They instead describe a wavefield that forward propagates from $\mathbf{x}_A$, positioned just beneath the free-surface, until it reaches the open triangle at $\mathbf{x}_B$ on the right-hand side

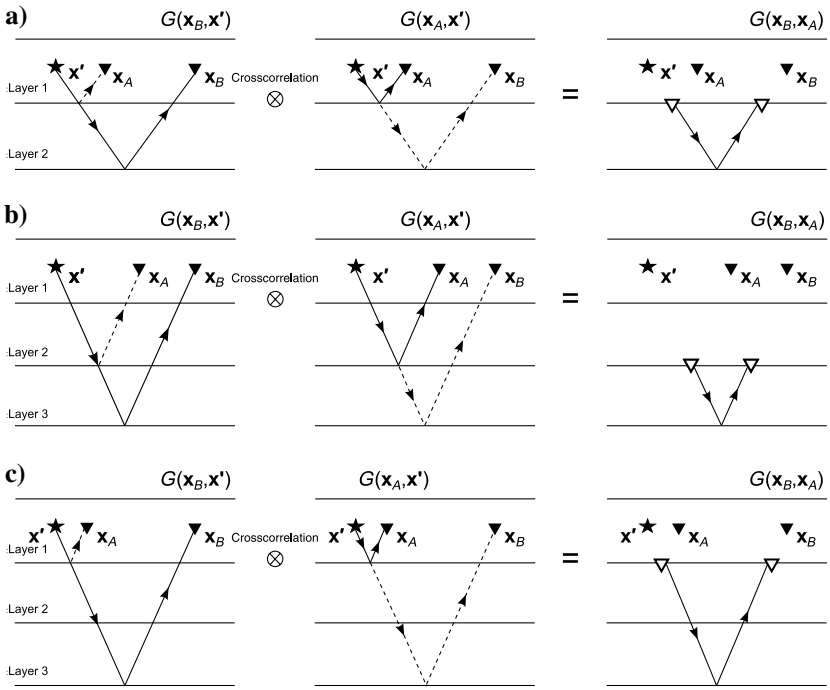

Figure 2. Nonphysical reflections in crosscorrelational seismic interferometry. (a) Crosscorrelation of the primary reflection from the second interface at $\mathbf{x}_B$ (left) with the primary reflection from the first interface at $\mathbf{x}_A$ (middle) isolates a nonphysical reflection from the second interface (right), as though the virtual source and receiver were positioned at the first interface (open triangles). (b) Crosscorrelation of the primary reflection from the third interface at $\mathbf{x}_B$ (left) with the primary reflection from the second interface at $\mathbf{x}_A$ (middle) isolates a nonphysical reflection from the third interface (right), as though the virtual source and receiver were positioned at the second interface (open triangles). (c) Crosscorrelation of the primary reflection from the third interface at $\mathbf{x}_B$ (left) with the primary reflection from the first interface at $\mathbf{x}_A$ (middle) isolates a nonphysical reflection from the third interface (right), as though the virtual source and receiver were positioned at the first interface (open triangles).

of Figure 2. At this point, the wavefield bends negatively at the interface and backward propagates to $\mathbf{x}_B$ located just underneath the free-surface (see Figure 3 from Ikelle et al., 2009). This interpretation does not assume lateral invariance and also has the advantage that nonphysical reflections lie along the surface (i.e., the plane of integration used in crossconvolutional interferometry discussed next). The difference is that Ikelle et al. (2009) isolate the virtual event between a source at $\mathbf{x}_A$ and receiver at $\mathbf{x}_B$ by crosscorrelating different pairs of Green's functions. Here, however, we compute the Green's function between two receivers using a one-sided source array. This means that the resultant Green's function estimate samples a portion of the subsurface adjacent to the receiver pair.

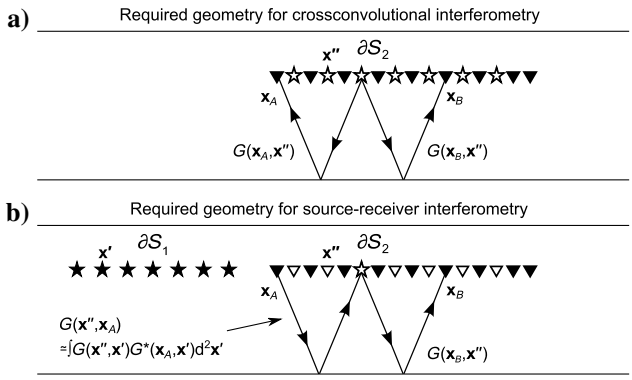

Figure 3. Acquisition geometries required for crossconvolutional (a) and source-receiver interferometry (b). The traveltime of the Green's function $G(\mathbf{x}_A, \mathbf{x}'')$ required by crossconvolutional interferometry (a) is equivalent to the traveltime of the Green's function $G(\mathbf{x}'', \mathbf{x}_A)$ obtained using crosscorrelational interferometry (b). The ∂S_1 and the ∂S_2 represent the source boundaries from crosscorrelational and crossconvolutional interferometry, respectively. For simplicity, we ignore free-surface effects in the sketch.

While crosscorrelational interferometry subtracts the traveltimes of the two recorded wavefields, crossconvolutional interferometry adds the traveltimes of the two wavefields. For example, given a source positioned midway between two receivers the crossconvolution of two appropriately chosen primary reflections, one propagating forward and one propagating backward, isolates the traveltime of a first-order free-surface multiple. To obtain the crossconvolutional Green's function we remove the complex conjugate from equation 1:

$$G(\mathbf{x}_B, \mathbf{x}_A) \approx \oint_{\partial S_2} \frac{2}{\rho c} G(\mathbf{x}_B, \mathbf{x}'') G(\mathbf{x}_A, \mathbf{x}'') d^2\mathbf{x}''. \quad (2)$$

Equation 2 is the far-field acoustic approximation to crossconvolutional interferometry and is similar to the integral derived by Poletto and Wapenaar (2009) used to obtain the Green's function as though there had been a reflector at the source boundary. Now it is necessary that receiver $\mathbf{x}_A$ is positioned outside of the source boundary (Figure 3a). Unfortunately, in marine exploration seismology it is unlikely that we have access to a receiver towed in front of the source at $\mathbf{x}_A$. However, we can circumvent this by constructing the forward-time Green's functions $G(\mathbf{x}'', \mathbf{x}_A)$ using crosscorrelational interferometry with the source boundary ∂S_1 (Figure 3b):

$$G(\mathbf{x}'', \mathbf{x}_A) + G^*(\mathbf{x}'', \mathbf{x}_A) \approx \oint_{\partial S_1} \frac{2}{\rho c} G(\mathbf{x}'', \mathbf{x}') G^*(\mathbf{x}_A, \mathbf{x}') d^2\,\mathbf{x}'. \quad (3)$$

By source-receiver reciprocity, the Green's function $G(\mathbf{x}'', \mathbf{x}_A)$ on the left-hand side of equation 3 are equivalent to those required by crossconvolutional interferometry as sketched in Figure 3a.

Substituting only the forward-time (t_+) Green's functions $G(\mathbf{x}'', \mathbf{x}_A) = G(\mathbf{x}_A, \mathbf{x}'')$ obtained from equation 3 into the crossconvolutional equation 2 we obtain the Green's function between receivers positioned at $\mathbf{x}_A$ and $\mathbf{x}_B$;

$$G(\mathbf{x}_B, \mathbf{x}_A) \approx \frac{4}{\rho^2 c^2} \int_{\partial S_2} \int_{\partial S_1} \times [G(\mathbf{x}'', \mathbf{x}') G^*(\mathbf{x}_A, \mathbf{x}')]_{t_+} \times G(\mathbf{x}_B, \mathbf{x}'') d^2\,\mathbf{x}' d^2\mathbf{x}''. \quad (4)$$

The outer integral assumes that sources and receivers are colocated on the boundary ∂S_2. We do not explicitly include it here, but convolution

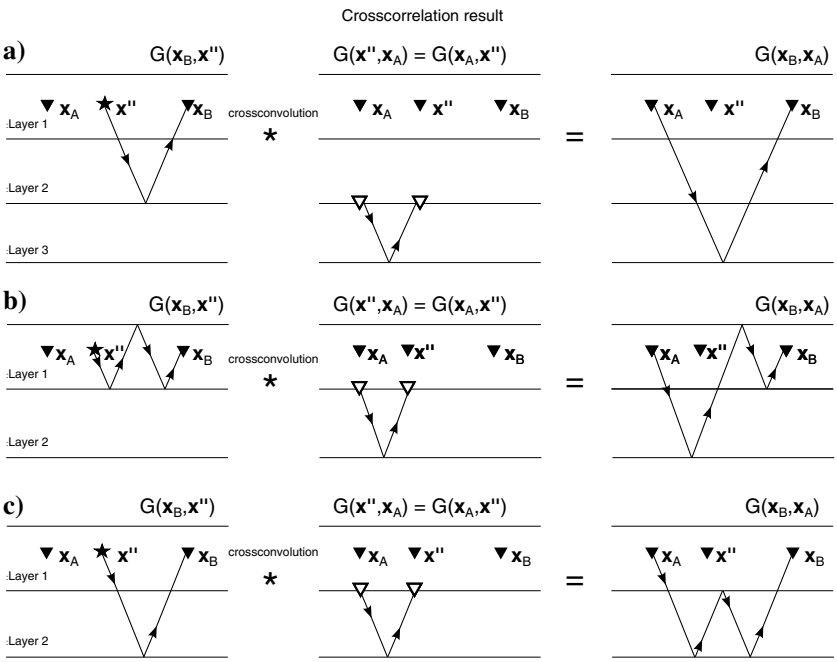

Figure 4. The construction of physical reflections using nonphysical reflections in source-receiver interferometry. (a) Crossconvolution of the primary reflection from the second interface (left) with the nonphysical reflection from the third interface as though the virtual source and receiver were positioned at the second interface (middle) isolates the primary reflection from the third interface. (b) Crossconvolution of a free-surface multiple (left) with the nonphysical reflection from the second interface as though the virtual source and receiver were positioned at the first interface (middle) isolates the free-surface multiple between receiver locations (right). (c) Crossconvolution of the primary reflection from the second interface (left) with the nonphysical reflection from the second interface as though the virtual source and receiver were positioned at the first interface (middle) isolates the internal multiple between receiver locations (right).

in equation 4 would result in $|s(\omega)|^2 s(\omega)$ being introduced on the right-hand side. Equation 4 represents an approximation to acoustic source-receiver interferometry.

An interesting aspect about source-receiver interferometry is that the nonphysical reflections created by crosscorrelational interferometry in the first step (square brackets in equation 4) contribute to the traveltime of physical reflections when convolved with the reflected Green's functions $G(\mathbf{x}_B, \mathbf{x}'')$ in the second step. We demonstrate this in Figure 4 which shows the construction of a primary reflection, free-surface multiple and an internal multiple in source-receiver interferometry using nonphysical reflections in a laterally invariant medium. For example, the traveltime of the primary reflection from the third interface is recovered by convolving the nonphysical reflection previously obtained by crosscorrelational interferometry in Figure 2b, with the primary reflection from the second interface (Figure 4a). Similar combinations between primaries and nonphysical reflections provide the traveltime of the other primary reflections (Ikelle et al., 2009).

In the derivation of equation 4, we used crosscorrelational interferometry to solve the problem of never having a receiver in front of the source (equation 3). At first, this step would seem unnecessary because in a 1D medium the corresponding physical Green's functions could be replicated by simply choosing the appropriate source to receiver offset. We instead use crosscorrelational interferometry because the purpose of this paper is to show how nonphysical reflections synthesized by that method can be combined to create physical reflections by using convolution.

Equation 4 appears similar to that derived in source-receiver interferometry (see equation 10 in Curtis and Halliday, 2010b). However, in principle, the two equations are different: in equation 4 we obtain the Green's function between two receivers using two source boundaries, whereas Curtis and Halliday (2010b) retrieve the Green's function between a source and receiver using two boundaries, one of sources and another of receivers. Curtis and Halliday (2010b) adopt the following approach: In the first step, the Green's functions between the receiver and the receivers on the boundary are obtained from crossconvolutional interferometry using Green's functions from a boundary of sources. This creates a virtual source at the receiver location alongside the original source. In the second step, the desired Green's function between the source and virtual source (previously the receiver) is obtained from crosscorrelational interferometry using recordings at the receiver boundary. The term source-receiver interferometry is entirely appropriate for equation 4 because in the first step we turn a receiver into a virtual source using crosscorrelational interferometry and in the second step, we convolve the virtual source recordings with recordings at the other receivers using a second source boundary.

Equation 4 is similar to that used by Ikelle et al. (2009) and Poletto and Farina (2010) to predict internal multiples and free-surface multiples, respectively. The former authors select appropriate combinations of primary reflections to predict internal multiples similar to that shown in Figure 4c. The latter authors use physical reflections obtained by crosscorrelational interferometry to predict free-surface multiples by crossconvolution.

ILLUSTRATIVE EXAMPLE

Figure 5 shows an acoustic three-layered velocity model and acquisition geometry. The full wavefield from each source (stars) to all receivers (triangles) was modeled modeled using a finite-difference scheme (Robertsson et al., 1994). For each source we subtract the modeled direct arrival from the full wavefield to obtain only the reflected wavefield at the receivers.

Figure 6a shows the Green's function estimates obtained using equation 1 by crosscorrelating the reflected wavefield at receiver r_1 ($\mathbf{x}_A$) with itself and with the reflected wavefield along the receiver array, and summing the crosscorrelations over the source boundary ∂S_1. Arrowheads (1–4) annotate the dominant nonphysical reflections. Nonphysical reflection (1) is created by the crosscorrelation of the primary reflection from the second interface with the primary reflection from the first interface (e.g., Figure 2a). Nonphysical reflection (2) is created by the crosscorrelation of the primary reflection from the third interface with the primary reflection from the second interface (e.g., Figure 2b). The crosscorrelation between the primary reflection from the third interface and primary reflection from the first interface as sketched in Figure 2c provides nonphysical reflection (3). Nonphysical reflection (4) is less intuitive, but is provided by the crosscorrelation of the primary reflection from the third interface with the first-order free-surface multiple. Figure 6b shows the Green's function estimates obtained using source-receiver interferometry in equation 4. The waveforms are broader than those obtained using crosscorrelational interferometry because the convolution of the source wavelet is introduced on the

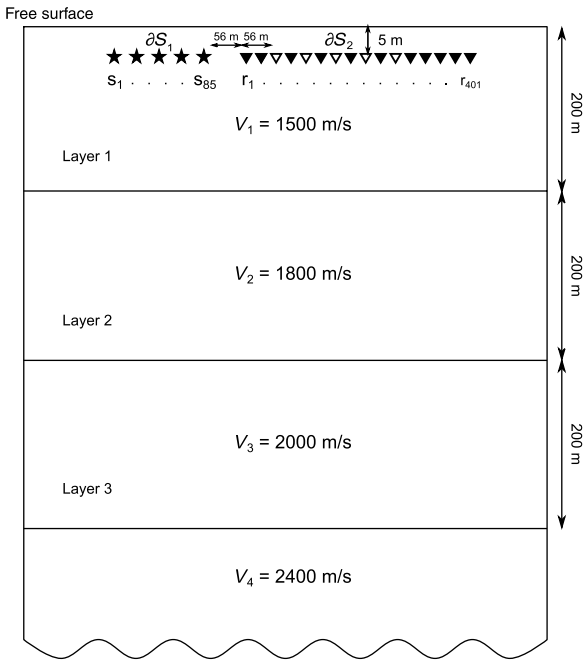

Figure 5. Three-layer acoustic velocity model and acquisition geometry. The source boundary ∂S_1 contains 85 sources (stars), separated at 8-m intervals, and illuminates 401 receivers (triangles) separated at 4-m intervals. Open triangles represent colocated receivers and sources corresponding to the ∂S_2 boundary, which also contains 85 sources (or 85 receivers). Sources and receivers are positioned at 5-m depth. The interval velocities V_k, are shown for the kth layer, where $k = 1, \ldots, 3$.

right-hand side of equation 4. The near-offsets are missing in Figure 6b because the first convolution is between the receiver at $\mathbf{x}_A$ (i.e., r_1) and the receiver at $\mathbf{x}_B$, which is positioned 56 m from the first source on ∂S_2 in equation 4. For comparison, Figure 6c shows the gather as if an actual source was positioned at r_1.

By using source-receiver interferometry, we obtain Green's functions that more closely resemble the true Green's functions (Figure 6c) and which show fewer nonphysical reflections than the Green's function estimates made using crosscorrelational interferometry (Figure 6a). As described above, it appears that nonphysical reflections produced in crosscorrelational interferometry provide physical reflections in source-receiver interferometry. This is important because the primary reflections and internal multiples cannot be retrieved by the crossconvolutions of physical reflections from an upper source boundary (e.g., equation 2). They can only be retrieved using appropriate convolutions of primary reflections and nonphysical reflections in source-receiver interferometry (e.g., equation 4). For example, the primary reflection from the second interface (P2) in Figure 6b is provided by the convolution of nonphysical reflection (1) in Figure 6a with the primary reflection from the first interface. Likewise, the primary reflection from the third interface (P3) is provided by the convolution of nonphysical reflection (2) in Figure 6a with the primary reflection from the second interface (e.g., Figure 4a). These dominant nonphysical reflections have been used to create physical reflections by source-receiver interferometry.

The convolution of pairs of physically reflected wavefields results in physical free-surface multiples in a laterally invariant medium. The convolutions of nonphysical reflections with multiples as shown in Figure 4b enhances these free-surface multiple estimates in source-receiver interferometry. However, it should be remembered there still exist convolutions that will provide nonphysical reflections after source-receiver interferometry (e.g., see arrivals at the white arrowheads in Figure 6b). Despite this, their amplitudes are much weaker than the corresponding nonphysical reflections from crosscorrelational interferometry.

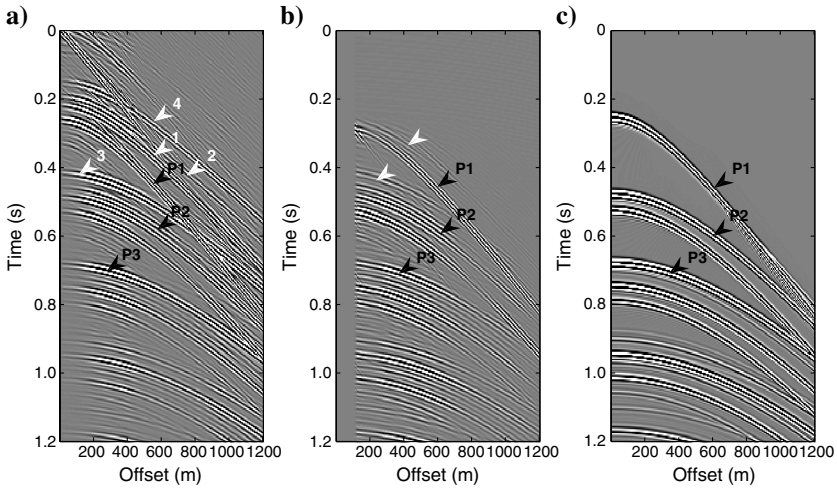

Figure 6. Green's function estimates obtained using (a) crosscorrelational interferometry (equation 1) and (b) source-receiver interferometry (equation 4). (c) True Green's functions. White arrowheads (1–4) in (a) denote nonphysical reflections (explained in text). P1–P3 denote primary reflections from the first, second and third interface, respectively.

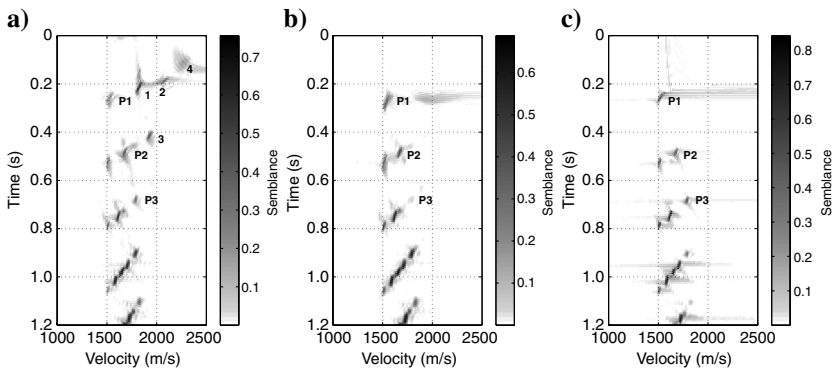

Figure 7. (a, b, and c) The velocity spectrum obtained from the Green's functions in Figure 6a, 6b, and 6c, respectively. Annotated peaks correspond to the arrivals in Figure 6.

Identifying the nonphysical reflections from physical reflections is an important issue. Draganov et al. (2010) show that unlike their physical counterparts, nonphysical reflections are identifiable because they change polarity after application of a damping compensation factor to the Green's function estimates. Curtis and Halliday (2010a) show that the nonphysical arrivals can be identified by using either wavefield separation or by reversing the order of the crosscorrelation in perturbed acoustic media (physical arrivals obey reciprocity, nonphysical arrivals do not).

We can also use source-receiver interferometry as a tool to identify the dominant nonphysical reflections produced in crosscorrelational interferometry. We can discriminate the nonphysical reflections easily by transforming the gathers into the time-velocity domain, or in other words, by generating their velocity spectra. The velocity spectrum displays the signal coherency along hyperbolic traveltimes t according to the equation,

$$t = \sqrt{t_0^2 + \frac{x^2}{V^2}}, \tag{5}$$

where t_0 is the two-way zero-offset traveltime, x is the offset between the virtual source and receiver, and V is the velocity of the subsurface (Taner and Koehler, 1969). We adopt semblance as the coherency measure (Neidell and Taner, 1971; King et al., 2011; Poliannikov and Willis, 2011; Mikesell and van Wijk, 2011), which is defined as

$$S_c = \frac{E_{\text{out}}}{M \cdot E_{\text{in}}} \qquad 0 \le S_c \le 1, \tag{6}$$

where

$$E_{\text{out}} = \sum_{t=t(i)-\Delta t/2}^{t=t(i)+\Delta t/2} \left\{ \sum_{i=1}^{M} f_{i,t} \right\}^2, \tag{7}$$

and

$$E_{\text{in}} = \sum_{t=t(i)-\Delta t/2}^{t=t(i)+\Delta t/2} \sum_{i=1}^{M} f_{i,t}^2, \tag{8}$$

where M is equal to the number of traces, $t(i)$ is the traveltime (equation 5), $f_{i,t}$ is the amplitude value on the jth trace at time t and offset $x(j)$, and Δt is a time-window equal to 8 ms in the following example.

Figure 7a shows the velocity spectrum obtained from the Green's functions in Figure 6a while Figure 7b shows that obtained from the Green's functions in Figure 6b. Although the waveforms are different in Figure 6a and 6b, this does not affect the velocity analysis using equation 5. Figure 7c shows the spectrum obtained from the true Green's functions in Figure 6c. Peaks corresponding to nonphysical reflections 1, 2, 3, and 4 in Figure 7a are suppressed in Figure 7b. The peak to the right of P1 in Figure 7b represents the nonphysical reflection prior to the corresponding primary in Figure 6b. Nevertheless, the velocity spectrum obtained from the source-receiver interferometric Green's functions shows good resemblance with the true velocity spectrum. Therefore, the velocity spectrum from source-receiver interferometry can be used in comparison with the velocity spectrum from crosscorrelational interferometry to help identify the dominant nonphysical reflections, in this case nonphysical reflections 1, 2, and 3.

Furthermore, the nonphysical reflections in crosscorrelational interferometry can also be used to characterize the interval velocities of the model. Consider again the nonphysical reflection created by the crosscorrelation of the primary reflections in Figure 2a. If this specific crosscorrelation were to be repeated using a linear array of sources like that shown in Figure 5 to obtain the Green's functions along a receiver array, we would expect the nonphysical reflection to moveout with the interval velocity V_2 and have a zero-offset traveltime $t_{02} = 2Z_2/V_2$, where Z_2 is the thickness of the second layer. Similarly, the crosscorrelation between the primary reflection from the third interface with the primary reflection from the second interface provides the traveltime of a nonphysical reflection with moveout of the interval velocity V_3 and has a zero-offset traveltime $t_{03} = 2Z_3/V_3$, corresponding to a reflection propagating through the third layer only (Figure 2b). In general, the interval velocity V_k and two-way traveltime t_{0k} of the kth layer can be extracted by crosscorrelating the primary reflections from the top and bottom of the kth layer along a receiver array. These nonphysical reflections will be identifiable because the traveltime propagating through a single layer has the smallest t_0 traveltime. We exploit this property to find the interval velocities and thicknesses from the Green's function estimates in Figure 6a.

Figure 8 shows the velocity spectrum in Figure 7a between 0 and 0.35 s. As expected, the nonphysical peaks that have the smallest traveltimes correspond to the nonphysical reflections described above (e.g., Figure 2a and 2b).

We are able to determine both interval velocity and layer thickness for each layer using the physical reflection P1, and nonphysical reflections 1 and 2. The interval velocity and corresponding thickness parameters (computed using the relation $Z_k = (t_{0k}V_k)/2$) in Figure 8 show good agreement with the model values in Figure 5.

ITERATIVE EXAMPLE

The procedure in equation 4 involves a double integral over three sets of Green's functions. In principle, the theory of source-receiver interferometry imposes no constraint on the number of crosscorrelational/crossconvolutional boundaries and integrations. We now investigate what happens when we include a further crossconvolution on the right-hand side of equation 4. Mathematically, the above statement corresponds to a triple integral:

$$G(\mathbf{x}_B, \mathbf{x}_A) \approx \frac{8}{\rho^3 c^3} \int_{\partial S_2} \int_{\partial S_2} \int_{\partial S_1} [G(\mathbf{x}'', \mathbf{x}') G^*(\mathbf{x}_A, \mathbf{x}')]_{t+} \times G(\mathbf{x}_B, \mathbf{x}'') G(\mathbf{x}_B, \mathbf{x}'') d^2\mathbf{x}' d^2\mathbf{x}'' d^2\mathbf{x}'', \tag{9}$$

where we include a further crossconvolution of the Green's functions $G(\mathbf{x}_B, \mathbf{x}'')$ and integration along the source boundary ∂S_2 on the right-hand side. On the right-hand side, the source wavelet contribution becomes $|s(\omega)|^2 s(\omega) s(\omega)$. In the 1D example, the procedure can be thought of as convolving the source-receiver interferometric Green's function estimates in Figure 6b with the physical Green's functions and integrating again over the source boundary ∂S_2.

Figure 9a shows the Green's function estimates obtained using the original form of source-receiver interferometry (equation 4) and is identical to that shown previously in Figure 6b. Figure 9b shows the Green's function estimates obtained using a new form of source-receiver interferometry (equation 9 and Figure 9c display the true Green's functions. It is clear from Figure 9b, that higher-order reflections are recovered by introducing a further convolution. The white arrowhead above the first-order free-surface multiple (M1) highlights a remaining nonphysical reflection. This arrival is created by convolution of the upper nonphysical reflection in Figure 9a with the physical primary reflection from the first interface. Despite this, the lower nonphysical reflection in Figure 9a has been used again to a create physical reflection. The lower nonphysical reflection in Figure 9a is equivalent to nonphysical reflection

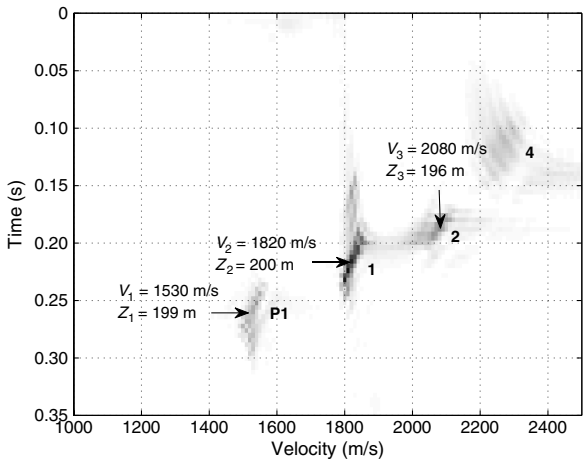

Figure 8. A close-up of the velocity spectrum in Figure 7a showing peaks between 0–0.35 s. These peaks allow for a layer velocity and thickness interpretation as shown.

(3) in Figure 2c and Figure 6a. When this nonphysical arrival is convolved with the primary reflection from the first interface in equation 9, we recover the primary reflection from the third interface (P3) in Figure 9b. Thus, it would appear that by using a further convolution in equation 9, we can suppress some of the remaining nonphysical reflections by using them to provide the true reflections at later times.

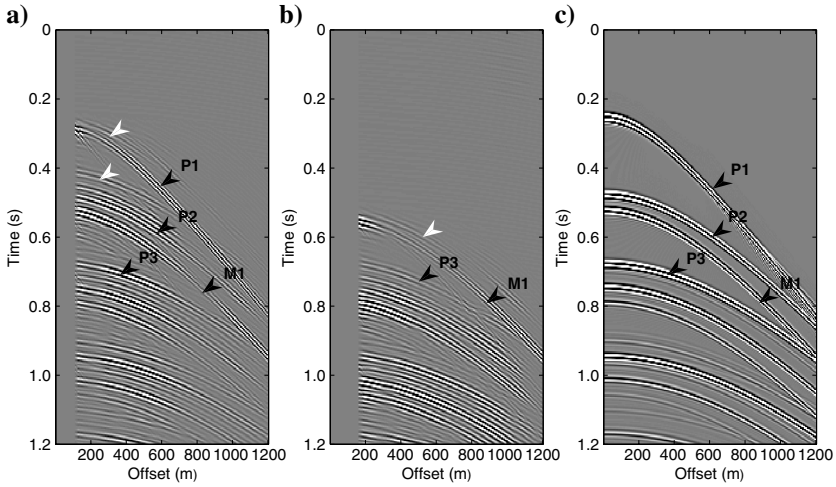

Figure 9. Green's function estimates obtained using (a) the original form of source-receiver interferometry (equation 4) and (b) a new form of source-receiver interferometry (equation 9). (c) True Green's functions. The arrows P1–P3 denote primary reflections from the first, second, and third interface, respectively; M1 corresponds to the first-order free-surface multiple and white arrowheads correspond to nonphysical reflections.

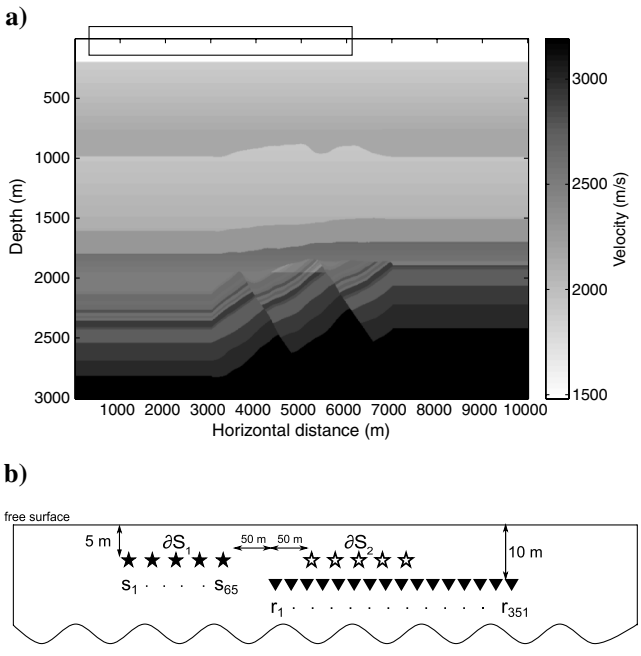

Figure 10. (a) A 2.5D elastic North Sea model. (b) Acquisition geometry located within the confines of the box in (a). Source boundaries ∂S_1 and ∂S_2 contain 65 sources separated at 25-m intervals. The 351 receivers are separated at 12.5-m intervals.

DISCUSSION

There are several limitations to the velocity analysis procedure described above. Unlike the primary reflections, nonphysical reflections do not propagate directly between the two receivers. The nonphysical reflection samples a portion of the subsurface left (or right) of the receivers (e.g., Figure 2a). In a medium with lateral velocity variations, the estimated seismic velocity will be inaccurate if the seismic velocity through which the nonphysical reflection has traveled is different than the desired seismic velocity directly underneath the receivers. Additionally, while the above example is acoustic, in the (an)elastic real earth, mode conversions between P- and S-waves are likely to complicate velocity interpretations.

We investigate the above limitations by comparing crosscorrelational and source-receiver interferometry for the 2.5D elastic North Sea model in Figure 10a. Source boundaries ∂S_1 and ∂S_2, each containing 65 sources, and 351 receivers are positioned as shown in Figure 10b. Sources and receivers are vertically offset by 5 m. This contravenes the requirement in source-receiver interferometry that sources and receivers are colocated on the boundary ∂S_2 (Figure 3b). In this instance the depth difference is small and we do not correct for this discrepancy.

Figure 11a shows the Green's function estimates obtained using crosscorrelational interferometry (equation 1), with the virtual source positioned at r_1, Figure 11b shows the Green's function estimates obtained using source-receiver interferometry (equation 4), and Figure 11c shows the true Green's functions. Similar to before, the waveforms are broader than those from crosscorrelational interferometry due to the convolution of the Green's function and its source wavelet. We identify two nonphysical reflections (annotated by white arrowheads in Figure 11a) obtained by crosscorrelational interferometry, which are suppressed by source-receiver interferometry. Furthermore, source-receiver interferometry does well at constructing the later arrival times. For example, the source-receiver interferometric Green's functions inside the ellipse at approximately 1.5 s show better resemblance to the true Green's functions than the corresponding crosscorrelational interferometric Green's functions.

Figure 12 show the corresponding velocity spectra for the Green's functions described above. We now use a time-window of length 12 ms around the traveltimes computed using equation 5. Peaks enclosed by the ellipses at approximately 0.5 s and 0.75 s in Figure 12a correspond to the two annotated nonphysical reflections in Figure 11a. No equivalent peaks exist inside the ellipses after source-receiver interferometry in Figure 11b. We identify a further nonphysical reflection at approximately 1.5 s in Figure 12a, which is also suppressed after source-receiver interferometry. Overall, the source-receiver interferometric velocity spectrum shows a better resemblance to the true velocity spectrum. These results suggest that source-receiver interferometry is more effective than crosscorrelational interferometry for surface seismic data.

While the subsurface seismic velocity interpretation in Figure 8 is straightforward for the acoustic model in Figure 5, the method has

limitations that are worth discussing when applied to a complex medium like that in Figure 10a. First, nonphysical reflections may be less identifiable in a complex medium. Draganov et al. (2010) shows that for a complex subsurface the nonphysical reflections will smear into correlation noise and hence, not appear as identifiable events. Similarly, we only identify three prominent nonphysical reflections in Figure 12 and a priori we cannot be confident that any of them provides the velocity and thickness of a specific layer. Assigning a velocity and thickness interpretation to these peaks is difficult because the nonphysical reflections are likely to represent a correlation between higher-orders of reflections.

In reality, assigning the peaks of nonphysical reflections to specific layers may prove problematic even in the acoustic scenario. In Figure 8 we assumed that a peak with an increased velocity represented a nonphysical reflection propagating through a deeper and therefore successive layer. If for example the velocity had decreased in one layer relative to the layer above, we would have interpreted the corresponding peak to have traveled through a shallower, but nonexistent layer. Furthermore, identifying the appropriate nonphysical reflections based on their t_0 traveltime will not always work. In Figure 8 we conveniently ignored nonphysical reflection (4) even though its t_0 traveltime was the smallest of the nonphysical reflections. Similarly, it is plausible that a nonphysical reflection which has traveled through two thinner layers (e.g., Figure 2c) has a smaller t_0 traveltime than a nonphysical reflection which has traveled through a single but thicker layer. In this instance, choosing the peaks which have the smallest t_0 traveltimes as above would lead to an inaccurate estimation of velocity. Thus, it would appear that any velocity estimate made using nonphysical reflections would need to be confirmed or verified by conventional methods. Nevertheless, the information provided by the nonphysical reflections clearly contains complementary information.

The source at $\mathbf{x}'$ in Figure 2a provides the dominant contribution to the retrieval of the nonphysical reflection and is therefore referred to as a stationary-phase source (Snieder et al., 2006). Hence, to recover a nonphysical reflection that has the correct velocity and traveltime requires sources to be positioned at the *nonphysical* stationary-phase locations. If the stationary-phase sources are missing, the nonphysical reflections will have inaccurate traveltimes and velocities in much the same way that the physical reflections may be poorly constructed if the appropriate stationary-phase sources are not sampled.

Interestingly, Mallinson et al. (2011) show that a physical refraction can be created using a similar method to that outlined here. In the first step, the authors crosscorrelate two refractions which leads to a nonphysical arrival termed the virtual refraction (Mikesell et al., 2009). The virtual refraction passes through the origin of the virtual source gather and has a linear moveout that defines the velocity of the refracting medium. Like the nonphysical reflection, the virtual refraction appears to be acquired with the virtual source and receiver positioned on the refracting interface. In the second step, Mallinson et al. (2011) convolve the virtual refraction with a physical refraction from the same interface. This step creates a physical refraction by, in effect, adding the upgoing and downgoing component to the virtual refraction. Similarly, we have used a crosscorrelation and then convolution to convert a nonphysical reflection into a physical reflection.

Crosscorrelational interferometry using equation 1 forms the basis for interferometric imaging (Snieder, 2004) and interpolation schemes (Wang et al., 2009; Hanafy et al., 2009; Wang et al., 2010). In these applications the Green's functions suffer from nonphysical reflections caused by a limited source aperture. Source-receiver interferometry may suppress some of the nonphysical reflections in the resultant images and virtual source gathers.

Despite the various practical limitations outlined above, the theory presented shows why source-receiver interferometry might perform better than crosscorrelational and crossconvolutional interferometry in some situations. It also shows that nonphysical reflections contain physical information about the medium of propagation. Even though these methods have practical limitations in

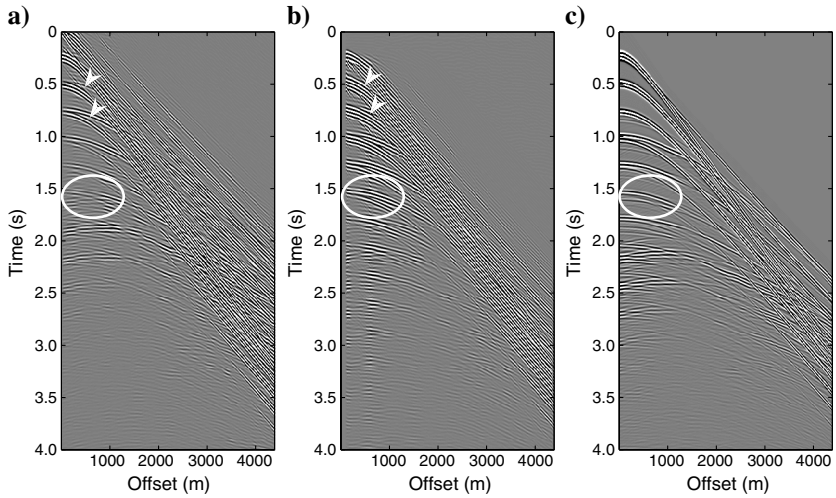

Figure 11. Green's function estimates obtained using (a) crosscorrelational interferometry (equation 1) and (b) source-receiver interferometry (equation 4). (c) True Green's functions.

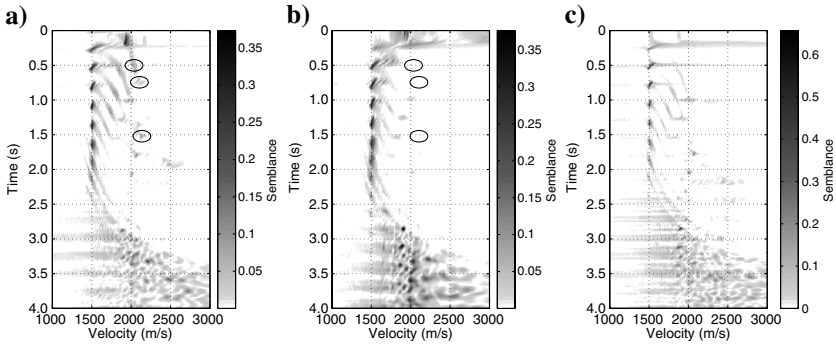

Figure 12. (a, b, and c) The velocity spectrum obtained from the Green's functions in Figure 11a, 11b, and 11c, respectively.

the laterally heterogeneous earth, it should be remembered that conventional moveout-based velocity analysis methods also share several such limitations. Hence, it is likely that in the future these methods may provide complementary information to conventional techniques, and that research into new methods to obtain physical information from nonphysical arrivals will be profitable.

CONCLUSION

Seismic interferometry refers to the process whereby the Green's function is synthesized between two receivers using their recordings from a surrounding and enclosing boundary of sources. If only surface sources are available, nonphysical reflections that represent the crosscorrelation of reflections from different interfaces are introduced into the Green's function estimates.

We show that nonphysical reflections can be used to our advantage: so-called source-receiver interferometry converts many of the nonphysical reflections obtained using crosscorrelational interferometry back into physical reflections via crossconvolutional interferometry. The resultant Green's function estimates display fewer nonphysical reflections than those obtained using crosscorrelational interferometry and display better agreement with the true Green's functions propagating between the receivers. We can use source-receiver interferometry to identify the dominant nonphysical reflections obtained from crosscorrelational interferometry. This can be achieved by transforming the crosscorrelational and source-receiver interferometric Green's functions into the time-velocity domain.

The nonphysical reflections obtained initially by crosscorrelational interferometry are particularly important in generating the primary reflections and internal multiples via convolution. This is because the primary reflections and internal multiples cannot be retrieved by the convolution of physical reflections from surface sources, but only by the appropriate convolution of a nonphysical and physical reflection. We demonstrate crosscorrelational and source-receiver interferometry on a 1D acoustic and a 2.5D elastic model, respectively. In the 1D example, we show that nonphysical reflections associated with the crosscorrelation of the primary reflection from the top and bottom of a specific layer allow for the direct estimation of interval velocities and layer thicknesses. Identifying the appropriate nonphysical reflection for velocity estimation is more difficult in the complex 2.5D example, but improvements in the Green's functions are still visible.

ACKNOWLEDGMENTS

We thank WesternGeco for permission to publish this work. The North Sea synthetic data set was generated as part of collaborative projects between Schlumberger, Lawrence Livermore National Laboratory, and Statoil. We thank Statoil for permission to show the synthetics and Schlumberger for permission to show the results. We acknowledge the support from the Scottish Funding Council for the ECOSSE Joint Research Institute with the Heriot-Watt University which is a part of the Edinburgh Research Partnership in Engineering and Mathematics (ERPem). The reviewers are thanked for their comments which helped to improve the manuscript.

REFERENCES

Bakulin, A., and R. Calvert, 2006, The virtual source method: Theory and case study: Geophysics, **71**, no. 4, SI139–SI150, doi: 10.1190/1.2216190.

Curtis, A., and D. Halliday, 2010a, Directional balancing for seismic and general wavefield interferometry: Geophysics, **75**, no. 1, SA1–SA14, doi: 10.1190/1.3298736.

Curtis, A., and D. Halliday, 2010b, Source-receiver wavefield interferometry: Physical Review E, **81**, 046601, doi: 10.1103/PhysRevE.81.046601.

Curtis, A., H. Nicolson, D. Halliday, J. Trampert, and B. Baptie, 2009, Virtual seismometers in the subsurface of the earth from seismic interferometry: Nature Geoscience, **2**, 700–704, doi: 10.1038/ngeo615.

Dix, C. H., 1955, Seismic velocities from surface measurements: Geophysics, **20**, 68–86, doi: 10.1190/1.1438126.

Draganov, D., R. Ghose, E. Ruigrok, J. Thorbecke, and K. Wapenaar, 2010, Seismic interferometry, intrinsic losses and Q-estimation: Geophysical Prospecting, **58**, 361–373, doi: 10.1111/(ISSN)1365-2478.

Duguid, C., D. Halliday, and A. Curtis, 2011, Source-receiver interferometry for seismic wavefield construction and ground roll removal: The Leading Edge, **30**, 838–843, doi: 10.1190/1.3626489.

Halliday, D., and A. Curtis, 2008, Seismic interferometry, surface waves and source distribution: Geophysical Journal International, **175**, 1067–1087, doi: 10.1111/gji.2008.175.issue-3.

Halliday, D., and A. Curtis, 2009, Generalized optical theorem for surface waves and layered media: Physical Review E, **79**, 056603, doi: 10.1103/PhysRevE.79.056603.

Hanafy, S. M., W. Cao, and G. T. Schuster, 2009, Interferometric interpolation of 3D SSP data: SEG, Technical Program Expanded Abstracts, **28**, 3138–3142.

Hong, T., and W. Menke, 2006, Tomographic investigation of the wear along the San Jacinto fault, southern California: Physics of the earth and Planetary Interiors, **155**, 236–248, doi: 10.1016/j.pepi.2005.12.005.

Ikelle, L. T., I. Erez, and X. Yang, 2009, Scattering diagrams in seismic imaging: More insights into the construction of virtual events and internal multiples: Journal of Applied Geophysics, **67**, 150–170, doi: 10.1016/j.jappgeo.2008.10.009.

King, S., A. Curtis, and T. L. Poole, 2011, Interferometric velocity analysis using physical and nonphysical energy: Geophysics, **76**, no. 1, SA35–SA49, doi: 10.1190/1.3521291.

Mallinson, I., P. Bharadwaj, G. Schuster, and H. Jakubowicz, 2011, Enhanced refractor imaging by supervirtual interferometry: The Leading Edge, **30**, 546–550, doi: 10.1190/1.3589113.

Mehta, K., A. Bakulin, J. Sheiman, R. Calvert, and R. Snieder, 2007, Improving the virtual source method by wavefield separation: Geophysics, **72**, no. 4, V79–V86, doi: 10.1190/1.2733020.

Mikesell, D., and K. van Wijk, 2011, Seismic refraction interferometry with a semblance analysis on the crosscorrelation gather: Geophysics, **76**, no. 5, SA77–SA82, doi: 10.1190/geo2011-0079.1.

Mikesell, D., K. van Wijk, A. Calvert, and M. Haney, 2009, The virtual refraction: Useful spurious energy in seismic interferometry: Geophysics, **74**, no. 3, A13–A17, doi: 10.1190/1.3095659.

Neidell, N. S., and M. T. Taner, 1971, Semblance and other coherency measures for multichannel data: Geophysics, **36**, 482–497, doi: 10.1190/1.1440186.

Poletto, F., and B. Farina, 2010, Synthesis and composition of virtual-reflector (VR) signals: Geophysics, **75**, no. 4, SA45–SA59, doi: 10.1190/1.3433311.

Poletto, F., and K. Wapenaar, 2009, Virtual reflector representation theorem (acoustic medium): Journal of the Acoustical Society of America, **125**, no. 4, EL111–EL116, doi: 10.1121/1.3081975.

Poliannikov, O. V., and M. E. Willis, 2011, Interferometric correlogram-space analysis: Geophysics, **76**, no. 1, SA9–SA17, doi: 10.1190/1.3519875.

Robertsson, J. O. A., J. O. Blanch, and W. W. Symes, 1994, Viscoelastic finite-difference modeling: Geophysics, **59**, 1444–1456, doi: 10.1190/1.1443701.

Schuster, G. T., J. Yu, J. Sheng, and J. Rickett, 2004, Interferometric/daylight seismic imaging: Geophysical Journal International, **157**, 838–852, doi: 10.1111/gji.2004.157.issue-2.

Slob, E., D. Draganov, and K. Wapenaar, 2007, Interferometric electromagnetic Green's functions representations using propagation invariants: Geophysical Journal International, **169**, 60–80, doi: 10.1111/gji.2007.169.issue-1.

Slob, E., and K. Wapenaar, 2007, Electromagnetic Green's functions retrieval by cross-correlation and cross-convolution in media with losses: Geophysical Research Letters, **34**, L05307, doi: 10.1029/2006GL029097.

Snieder, R., 2004, Extracting the Green's function from the correlation of coda waves: A derivation based on stationary phase: Physical Review E, **69**, 046610, doi: 10.1103/PhysRevE.69.046610.

Snieder, R., 2007, Extracting the Green's function of attenuating heterogeneous acoustic media from uncorrelated waves: Journal of the Acoustical Society of America, **121**, 2637–2643, doi: 10.1121/1.2713673.

Snieder, R., K. Wapenaar, and K. Larner, 2006, Spurious multiples in seismic interferometry of primaries: Geophysics, **71**, no. 4, SI111–SI124, doi: 10.1190/1.2211507.

Taner, M. T., and F. Koehler, 1969, Velocity spectra-digital computer derivation applications of velocity functions: Geophysics, **34**, 859–881, doi: 10.1190/1.1440058.

van der Neut, J., J. Thorbecke, K. Mehta, E. Slob, and K. Wapenaar, 2011, Controlled-source interferometric redatuming by crosscorrelation and multidimensional deconvolution in elastic media: Geophysics, **76**, no. 4, SA63–SA76, doi: 10.1190/1.3580633.

van Manen, D.-J., A. Curtis, and J. O. A. Robertsson, 2005, Modeling of wave propagation in inhomogeneous media: Physical Review Letters, **94**, 164301, doi: 10.1103/PhysRevLett.94.164301.

van Manen, D.-J., A. Curtis, and J. O. A. Robertsson, 2006, Interferometric modeling of wave propagation in inhomogeneous elastic media using time reversal and reciprocity: Geophysics, **71**, no. 4, SI47–SI60, doi: 10.1190/1.2213218.

van Wijk, K., 2006, On estimating the impulse response between receivers in a controlled ultrasonic experiment: Geophysics, **71**, no. 4, SI79–SI84, doi: 10.1190/1.2215360.

Vasconcelos, I., and R. Snieder, 2008a, Interferometry by deconvolution: Part 1 — Theory for acoustic waves and numerical examples: Geophysics, **73**, no. 3, S115–S128, doi: 10.1190/1.2904554.

Vasconcelos, I., and R. Snieder, 2008b, Interferometry by deconvolution: Part 2 — Theory for elastic waves and application to drill-bit seismic imaging: Geophysics, **73**, no. 3, S129–S141, doi: 10.1190/1.2904985.

Wang, Y., S. Dong, and Y. Luo, 2010, Model-based interferometric interpolation method: Geophysics, **75**, no. 6, WB211–WB217, doi: 10.1190/1.3505816.

Wang, Y., Y. Luo, and G. T. Schuster, 2009, Interferometric interpolation of missing seismic data: Geophysics, **74**, no. 3, SI37–SI45, doi: 10.1190/1.3110072.

Wapenaar, K., 2004, Retrieving the elastodynamic Green's function of an arbitrary inhomogeneous medium by cross correlation: Physical Review Letters, **93**, 254301, doi: 10.1103/PhysRevLett.93.254301.

Wapenaar, K., 2006, Green's function retrieval by cross-correlation in case of one-sided illumination: Geophysical Research Letters, **33**, doi: 10.1029/2006GL027747.

Wapenaar, K., and J. Fokkema, 2006, Green's function representations for seismic interferometry: Geophysics, **71**, no. 4, SI33–SI46, doi: 10.1190/1.2213955.

Wapenaar, K., J. van der Neut, and E. Ruigrok, 2008, Passive seismic interferometry by multidimensional deconvolution: Geophysics, **73**, no. 6, A51–A56, doi: 10.1190/1.2976118.

Wapenaar, K., J. van der Neut, E. Ruigrok, D. Draganov, J. Hunziker, E. Slob, J. Thorbecke, and R. Snieder, 2011, Seismic interferometry by crosscorrelation and by multidimensional deconvolution: A systematic comparison: Geophysical Journal International, **185**, 1335–1364, doi: 10.1111/gji.2011.185.issue-3.